Anna E. Clinger

Implications for post-comminution processes in subglacial suspended sediment using coupled radiogenic strontium and neodymium isotopes

Submitted for Publication in:

Geomorphology

in lieu of thesis in partial fulfillment of the requirements for the degree of
Master of Science in Earth and Environmental Sciences
Department of Earth and Environmental Sciences
The University of Michigan

Accepted by:

Signature	Name	Date
Signature	Sarah Aciego	Novmber 30, 2015
Signature	Rose Cory	1-Dec-2015
Department Chair Signature	Chris Poulsen	12/7/15

I hereby grant the University of Michigan, its heirs and assigns, the non-exclusive right to reproduce and distribute single copies of my thesis, in whole or in part, in any format. I represent and warrant to the University of Michigan that the thesis is an original work, does not infringe or violate any rights of others, and that I make these grants as the sole owner of the rights to my thesis. I understand that I will not receive royalties for any reproduction of this thesis.

☒ Permission granted.

☐ Permission granted to copy after: ________________

☐ Permission declined.

Author Signature

Earth and Environmental Sciences
UNIVERSITY OF MICHIGAN

Abstract

Enhanced physical weathering rates in subglacial systems promote high levels of comminution, transport, and deposition of fine-grained sediment within the subglacial drainage network. The impact of shifts in sediment loads due to variations in meltwater flux, and their effects on downstream ecosystems, remains poorly quantified and places a fundamental importance on our ability to characterize subglacial depositional environments. Here, for the first time, we assess the seasonal evolution of the subglacial suspended sediment using coupled radiogenic strontium ($^{87}Sr/^{86}Sr$) and neodymium ($^{143}Nd/^{144}Nd$) isotopic ratios with elemental ratios, and in-situ measurements. Weathering rates in fluvial and riverine systems have been traditionally assessed using radiogenic isotopic tracers: $^{143}Nd/^{144}Nd$ ratios relate to the crustal age whereas $^{87}Sr/^{86}Sr$ ratios relates to both age and preferential mineral dissolution. Relative shifts in these ratios allow us to characterize distinct sediment transport networks. We apply this technique to the Lemon Creek Glacier (LCG), Alaska, USA and the Athabasca Glacier (AG), Alberta, CA. At the LCG, the $^{143}Nd/^{144}Nd$ values range from ε_{Nd} of -4.6 (0.9) to -8.7 (0.2), which suggests a poorly mixed sediment flux. However, the greatest period of variability may correlate with the drainage of a supraglacial lake and suggests caution should be exerted in time-scale $^{143}Nd/^{144}Nd$ provenance studies that may be affected by climatic disturbances. In contrast, limited variation is observed within the AG $^{143}Nd/^{144}Nd$ seasonal record. A consistent, direct relation between the Rb/Sr elemental ratio and the $^{87}Sr/^{86}Sr$ ratio enables us to unravel incongruent weathering trends in the radiogenic Sr record. Correlation between the $^{87}Sr/^{86}Sr$ and total discharge suggests the process is partially controlled by mantling of the bedrock, which can be detected using post-comminution ages. While the subglacial structure may be enabled by the subglacial till beneath the AG, our study supports the use of Sr-Nd as a new proxy in the subglacial environment.

Keywords: Subglacial environment; radiogenic isotopes; suspended sediment; comminution;

1. Introduction

The predicted escalation of glacial retreat by the end of the twentieth century (IPCC, 2013) highlights the fundamental importance of quantifying how the environment is impacted by an increase in glacio-fluvial sediment deposition. In the subglacial hydrologic system, elevated pressures can promote the presence and motion of water at the base of the glacier. In turn, this meltwater flux facilitates the production and transfer of dissolved and suspended sediment (e.g. Collins, 1990), as well as significant physical and chemical weathering between bedrock and basal ice. Shifts in meltwater hydrochemistry and sediment load can have direct and profound influences on the nature of downstream ecosystems (e.g. Jacobsen et al., 2012; Muhlfeld et al., 2011; Xu et al., 2009). The impact of glacially derived sediment release is widely variable. For example, high sediment loads can disrupt salmon spawning grounds, whereas reductions in meltwater quality can destabilize benthic communities (Milner et al., 2009). Additionally, sediment flux can influence the degree and stability of channel distribution in pro-glacial riparian zones (Milner et al., 2009). Investigating the rate and scale at which sediment deposition, associated with hydrologic change, is occurring may provide insight into the sensitivity of downstream ecosystems to sediment flux.

While certain aspects of subglacial hydrology, such as water transit velocity, water quality, and subglacial water pressures, have been well studied (e.g. Anderson et al., 2004; Anderson, 2007; Brown, 2002; Hodge, 1976; Lamb et al., 1995; Moore et al., 2013; Stenborg, 1969; Tranter, 2005), the spatial distribution of the subglacial hydrological networks is less well constrained. In general, glaciers can be characterized by the annual presence of basal water. Cold-based temperatures glaciers generally lie below the pressure melting point throughout the entire year, whereas warm-based temperatures glaciers typically reach pressure melting point throughout the entire year, which promotes the presence of basal meltwater (e.g. Tranter, 2003). Poly-thermal glaciers exhibit both conditions per annum (e.g. Wadham et al., 1998). In systems where subglacial water is present, basal water is routed beneath glaciers and meltwater conduits can carve the glacial bedrock. These subglacial drainage systems can be classified into two categories: a distributed, slow-transit hydrologic system and a channelized, rapid-transit system (Raymond et al., 1995). However, subglacial systems cannot be defined seasonally or spatially by a single configuration, as the subglacial drainage network is constantly evolving (Fountain and Walder, 1998). In particular, dye-trace studies have revealed a hydrologic dispersion through the subglacial drainage network changes during the melt season where fast, efficient channels tend to dominate slow, inefficient networks as the melt season progresses and the subglacial drainage channels expand up-glacier (Bingham et al., 2005; Nienow et al., 1998). Hydrologic variability and glacial sedimentary output are directly linked; comminution of rock occurs as glacial ice physically abrades and meltwater chemically weathers the bedrock. Here, the resulting fresh and highly reactive sediment contributes to the dissolved and suspended sediment loads.

The geochemical behavior of glacially derived sediment has been increasingly studied over the past two decades (e.g. Brown et al., 1994; Hodgkins et al., 1995; Tranter et al., 1993; Tranter et al., 1995; Tranter et al., 2005). Yet, these limited number of studies, which characterize the subglacial depositional environment, have focused largely on the deformation of the glacial bed and till (e.g. Boulton et al., 2001; Evans et al., 2006;

van der Meer et al., 2003). Even fewer studies have addressed the seasonal dynamics of sediment entrainment, transport, and deposition in the subglacial environment (e.g. Alley et al., 1997; Collins, 1988; Lawson, 1993; Swift et al., 2002) or explored the coupled chemical-physical behavior of the subglacial sediment load (Brown et al., 1996).

If subglacial hydrological network processes mirror those of subaerial or riverine environments, they may exhibit similar depositional characteristics such as mantling of the bedrock or mineral sorting between grain sizes. Therefore the sediment depositional environment should also vary, like riverine environments, with location and lithology. But, glacial environments notably differ from riverine environments in that glacial abrasion leads to relatively high physical and low chemical weathering rates (Raiswell et al., 2006), a ratio that likely contributes defining characteristics to the sediment flux in the subglacial environment. The production of sediment through comminution processes leads to the exposure of fresh, reactive surfaces that can be deposited or excavated throughout the glacial system. While subglacial sediment deposition may simply be a function of the net sediment flux into a given subglacial area (Hart, 1995), entrainment occurs when a critical shear stress at the bed is exceeded (Walder and Fowler, 1994).

Further, during physical and chemical weathering processes, minerals entrained within the bedrock can be weathered both congruently and incongruently. Congruent weathering relates to processes involving the complete dissolution of minerals, whereas incongruent weathering relates to the conversion of an initial mineral into a secondary mineral through precipitation and dissolution processes. However, discerning the contribution of these two processes to the dissolved load and suspended sediments remains a challenge (e.g. Hindshaw et al., 2014), but the relative contributions may pose an interesting relationship if the sediment behaves in response to the high levels of comminution.

As tracers of source and weathering processes in fluvial environments, radiogenic isotopes have the potential for uncovering weathering and sediment transport processes within the subglacial environment. Weathering rates in fluvial and riverine systems have been assessed using radiogenic isotopic tracers (e.g. Derry and France-Lanord, 1996; Edmond, 1992).

Strontium isotope ($^{87}Sr/^{86}Sr$) fluxes have typically been analyzed in stream and river waters to trace mineral weathering reactions and rates and compare them to the isotopic characteristics of the underlying and local bedrock (e.g. Arn et al., 2003; Blum and Erel, 1995; Blum et al., 1993; Clow et al., 1997a; Stevenson et al., In review-b; Taylor and Blum, 1995). Due to the radiogenic decay of ^{87}Rb to ^{87}Sr, the $^{87}Sr/^{86}Sr$ ratio can also be used to place constraints on lithographic age. Radiogenic Sr is preferentially, incongruently, released from minerals such as biotite during periods of high weathering (e.g. Peucker-Ehrenbrink and Blum, 1998) . Potassium and calcium ions in minerals can readily substitute for Rb and Sr, respectively; therefore $^{87}Sr/^{86}Sr$ ratios in combination with elemental data can help discern differences in bedrock lithology (e.g. Krishnaswami et al., 1992). For example, carbonate-based catchments exhibit a relatively unradiogenic signature in comparison to silicate-based catchments, ($^{87}Sr/^{86}Sr = 0.708$ versus 0.721, respectively (Allègre et al., 2010)). The ratio may also de-convolve incongruent mineral weathering rates rock (e.g. Bain and Bacon, 1994; Capo et al., 1998; Clow et al., 1997b).

Neodymium isotopic ratios ($^{143}Nd/^{144}Nd$) have proven themselves as powerful tracers of dust transport, water mass, and sediment source (Aarons et al., 2013; Jiang et al., 2013; Jones et al., 1994; Piepgras and Jacobsen, 1988). Natural variation in the $^{143}Nd/^{144}Nd$ composition of rocks relates to the extent of mixing experienced by the material derived from the mantle from differently aged sources, which is enabled by the limited mobility of rare earth elements (REE), such as Sm and Nd, during sedimentary processes (Öhlander et al., 2014; Taylor and McLennan, 1995). Studies utilizing Nd as a tracer for intense chemical weathering are few, but pedogenic studies have shown intense weathering preferentially removes ^{143}Nd from soil profiles (Ma et al., 2010). However, Garçon et al. (2014) modeled the Nd composition of different minerals in sediment and found minerals highly enriched in Nd, notably monazite and alanine to dominate the Nd isotopic budgets, despite the mineral proportion consistently falling below 0.5% of the total rock weight. The study supports the general classification of Nd as a proxy for congruent weathering. Whilst still in development, the strength of the Nd proxy as a tracer of intensive chemical weathering may be supported by correlation with the more tested radiogenic isotope proxies of radiogenic strontium ($^{87}Sr/^{86}Sr$). Therefore, the relationship between radiogenic Nd and Sr systems has the potential to reveal dominant weathering mechanisms in subglacial environments.

By correlating the radiogenic Nd and Sr isotopic ratios with local geology, daily in-situ measurements and elemental data, we quantify the ability of this combined Sr-Nd proxy to track channel evolution and model weathering processes in subglacial environments. This study investigates for the first time the effectiveness of the application of coupled Sr-Nd ratios in suspended sediments from two distinct subglacial environments. Here we characterize the seasonal evolution of the subglacial meltwater channels from the Lemon Creek glacier (LCG), Juneau Icefield, Alaska and the Athabasca Glacier (AG), Columbia Icefield, Alberta.

2. Site Descriptions

2.1 Lemon Creek Glacier

The LCG is a warm-based valley glacier located in the Coast Mountain Range of southeast Alaska (11.6 km^2, 58° 24.418' N, 134° 22.379' W). The LCG forms the southernmost extension of the Juneau Icefield, which itself extends ~3,900 km^2. Annual mass balance surveys indicate that the glacier is retreating by an average of 0.48 m yr^{-1} of water equivalents (Miller and Pelto, 1999). Geologically, the LCG is located on a mid-Cretaceous metamorphic-pluton complex, with associated migmatites (Figure 1) (Brew and Ford, 1985; Kistler et al., 1993). Young tonalite sills (62-69 Ma, with a northeastward younging of the bedrock (Gehrels et al., 1984)) characterize the terrain to the immediate west and high-grade metamorphosed sedimentary and volcanic rocks characterize the surrounding area to the east. Late-Permian metamorphosed sedimentary (Greenschist facies) rocks characterize the area further west and beneath the glacial head (Kistler et al., 1993; Stevenson et al., In review-a). The local region maintains a maritime climate with average annual precipitation of 1.4 m yr^{-1} and mean winter and summer air temperatures of -1°C and 16°C, respectively (Stevenson et al., In review-b).

In a corresponding study, Stevenson et al. (In review-a) analyzed the radiogenic Sr isotopic compositions of the suspended sediment at the LCG. The time-series values ranged from $^{87}Sr/^{86}Sr$ = 0.708487(6) to 0.710003(8), for Julian Day (JD) 226—252. The study additionally includes measured radiogenic strontium values of four bedrock samples: quartzite ($^{87}Sr/^{86}Sr$ = 0.72960(1)), gneiss ($^{87}Sr/^{86}Sr$ = 0.70761(4)), plutonic igneous granodiorite ($^{87}Sr/^{86}Sr$ = 0.70710(4)), and a metamorphosed crystalline carbonate ($^{87}Sr/^{86}Sr$ = 0.70800(2)), with values in parentheses representing two standard error. The bedrock values align well with the radiogenic Sr ratios measured in the Juneau Gold Belt (Kistler et al., 1993). However, no measurements have characterized the radiogenic Nd compositions of the bedrock directly beneath the LCG. In a survey of the accretionary terranes of the Alaskan portion of the Coast Mountains, Samson et al. (1991) reported values from juvenile plutons (i.e. the Gravina belt and the Taku terrane) and metamorphic assemblages (i.e. the Tracy Arm, Endicott assemblage, Port Houghton assemblage, and the Ruth assemblage), but the wide range of $^{143}Nd/^{144}Nd$ values from 0.511290 ± 12 to 0.513030 ± 7 highlights need for direct bedrock measurements to characterize the local geology.

2.2 Athabasca Glacier

The Athabasca Glacier is one of the eight primary glaciers extending from the Columbia Icefield in the Canadian Rockies, Alberta (8.6 km^2, 52° 12.54' N, 117° 14.29' W). It is smaller than the Juneau Icefield spanning approximately 325 km^2. The icefield accumulates the largest volumes of snow and ice south of the Arctic Circle in the Northern Hemisphere and contributes freshwater to the Arctic, Pacific, and Atlantic Oceans (Paterson, 1964). The glacier itself spans over three icefalls and into a valley, is ~1950 m a.s.l, and extends ~6 km in length. Uplift and rotation define the regional geology, which is primarily Middle Cambrian limestone and shale (Figure 2) and part of the Pika Formation (Charlesworth and Erdmer, 1989). Beneath the ice, a thin (0.05-0.30 m) deformable layer of till exists which promotes till erosion, rotation, and detachment

(Hart, 2006). The Athabasca Glacier in particular has been the focus of many previous studies (e.g. Arendt et al., 2015; Kite and Reid, 1977; Paterson and Savage, 1963; Raymond, 1969; Xu et al., 2010). Like the LCG, the glacier has consistently decreased in total mass over the past decades of observation (Kite and Reid, 1977). In the past decade, the region has experienced 395 to 475 mm of annual precipitation and ranges of -15 to -19°C and +16 to +20°C winter and summer temperatures, respectively (Archive, 2013; Arendt et al., 2015; Shea and Marshall, 2007).

Similarly to the LCG, the bedrock provides a framework for isotopic analysis. The shales and limestones of the Pika Formation have been well-characterized as highly radiogenic by Boghossian et al. (1996), with ε_{Nd} of -27.1. However, the carbonate bedrock obstructs the possibility of measuring such radiogenic values within the strontium system. To a greater degree, the values from previous study (i.e. Millot et al., 2003) relate to weathering and preferential dissolution of carbonate and, in Athabasca River sediments, range from $^{87}Sr/^{86}Sr = 0.71285$ to 0.71612.

3. Sampling and Analysis

3.1 Sample collection

Samples were collected daily from the main meltwater channel draining the LCG from the 30th June 2012 to the 8th September 2012 (JD 182—252) and the AG from the 11th August 2014 to the 25th October 2014 (JD 223—298). The sampling site at the LCG shifted mid-season due to accessibility. From JD 182 to 210, sampling occurred from a 3 m snow pit where flowing water was observed. Once the seasonal snowpack decreased and the glacial toe was accessible, the sampling site was moved up-glacier 50 m closer to the glacier toe. Samples were collected at the second location daily from JD 227 to 252.

Ten liters of subglacial water were filtered using a Masterflex modular peristaltic pump and a Perfluoroether (PFA) 47mm diameter filtration unit (Savillex). Hydrophilic Polyvinylidene fluoride (PVDF) Millipore filter membranes (0.22 μm) were used to separate the suspended sediment.

Daily in-situ field protocols are outlined in (Stevenson et al., In review-b). In summary: Electrical conductivity, temperature, pH, dissolved oxygen (DO) and alkalinity measurements were taken using a YSI Handheld Multiparameter Instrument (Pro Plus Multiparameter). The electrical conductivity, temperature, and pH measurements were all conducted on-site in the subglacial outlet channels. Approximately 100 mL of filtered subglacial water was used for alkalinity measurements. For anticipated high alkalinities, the 100 mL sample was mixed with 10 mL of Total Alkalinity Reagent (FisherScientific) solution, shaken, and the pH measured. For anticipated low alkalinities, the 100 mL sample was mixed with 1 mL of Total Alkalinity Reagent solution, shaken, and the pH was measured. The pH was converted to the total alkalinity using a pH-total alkalinity conversion (e.g. Fujita, 2008; Hedin et al., 1994)

Two diurnal cycles were tracked at the AG. In August (JD 236—237), samples and in-situ measurements were collected every two hours. In October (JD 297—298) samples were collected every three hours due harsher field conditions.

3.2 Sample preparation

3.2.1 Lemon Creek suspended sediments

The samples were prepared for isotopic analysis in a class 10 laminar flow hood inside a 10,000 level clean room at the University of Michigan. Each filter membrane was rinsed with 18.1 MΩ cm to collect the sediment, which was subsequently dried in Teflon beakers. For the LCG samples, 10 mg of sediment were weighed and digested for 7 days in 2 mL concentrated nitric acid (HNO_3) with 0.5 mL concentrated hydrofluoric acid (HF). Samples were dried down and further digested in aqua regia for 24 hours to oxidize and remove any residual organic material. Each sample was digested in 1 mL aqua regia for 24 hours, dried on a hotplate, and dissolved in 1 mL of 9 M hydrochloric acid (HCl) in preparation for elemental separation.

3.2.2 Athabasca suspended sediments

Prior to dissolution procedures (above) the dry AG sediments were first filtered through a 0.63 μm sieve to eliminate potential effects of grain size distribution during fluvial transport. Approximately 10 mg of sediment were weighed and digested using Parr bombs. The sample was loaded into 3 mL Savillex beakers with 2 mL of concentrated HF. The beakers were placed in a 125 mL PTFE container and 6 mL of concentrated HF with trace concentrated HNO_3 was added. The vessel was enclosed in the Parr bomb and placed in a 220°C oven for 48 hours. The solutions were dried down on a hot plate and the procedure was replicated with 6 M HCl in both the Savillex beakers and PTFE container at 180°C for 12-16 hours. After the final dry-down, the samples were digested in 1 mL of 9 M HCl in preparation for elemental separation.

3.3 Elemental analysis of Athabasca Glacier samples

Trace and major elemental concentrations were measured in triplicate on the Thermo Scientific ELEMENT2 Inductively Coupled Plasma mass spectrometer at the University of Michigan Keck Laboratory in pulse counting mode. The digested sediment samples were acidified and diluted to 2 mL solutions. An acid blank and standard river reference standards were run every five samples to assess long-term reproducibility and accuracy. Repeat measurements of international standard NIST1640a are provided in Aciego et al., (2015). Baseline detection measurements from the total procedural blank indicate that analytical error was never greater than 10% the concentration even for the smallest concentrations. Such analyses were not possible for the LCG samples due to prior consumption of sample supply in earlier studies (Sheik et al., 2015).

3.4 Neodymium isotope analysis

Samples were aliquoted to obtain > 25 ng of Nd. Isolation of Nd was preformed through ion exchange column chemistry involving two columns. Each sample was first loaded into a 700 μL PFA column filled with 50-100 mesh TruSpec resin. Following the procedures of Aciego et al. (2009), HCl was used to elute high field strength elements (HFSE) and REEs. The eluted volumes were then loaded into a preconditioned 2 mL PFA column filled with clean 50-100 μm LnSpec resin. The subsequent volumes eluted with HCl isolated the Nd from the REE fraction (Aciego et al. 2009). An acid blank and a standard of known concentration (BCR-2) were processed using the same procedure to ensure long-term reproducibility and assess error.

Nd was loaded onto outgassed rhenium double filaments after 1 μL of 1 M HCl—1 M HNO_3 was added to each dried sample. A current of 0.8 A was run through the filament until the sample was dry. The current was slowly increased to 1.8 A and held constant for 1 minute. The current was then flashed at 2.2 A and decreased to 0 A.

Isotopic ratios were determined using a Thermo-Finnigan Triton Thermal Ionization Mass Spectrometer (TIMS) at the Glaciochemistry and Isotope Geochemistry Laboratory in the Department of Earth and Environmental Science at the University of Michigan (Aarons et al., 2013; Arendt et al., 2014). Instrumental mass bias was corrected for by applying an exponential mass fractionation law with the $^{146}Nd/^{144}Nd = 0.7219$ and mass 149 was monitored for Sm interference. Amplifier gains and baselines were run prior to each set of analysis. The Nd isotopic standard JNdi-1 (10 ng) was measured as $^{143}Nd/^{144}Nd = 0.512099 \pm 0.000016$ (2 s.d. n=8) which is in agreement with the accepted JNdi-1 standard value of $^{143}Nd/^{144}Nd = 0.512115$ (Tanaka et al., 2000). The $^{143}Nd/^{144}Nd$ of BCR-2 was 0.512643 ± 36 (2 s.d. in the last decimal place; n=5) and in agreement with the literature (Li et al., 2007; Raczek et al., 2003; Weis et al., 2006).

3.5 Strontium radiogenic isotope analysis

Radiogenic strontium values for suspended sediment were obtained from Stevenson et al., (In review-a). Here we expand their existing data set using the same analytical preparation and methods. In brief, samples were partitioned to provide 2 μg Sr, these aliquots were dried on a hot place and dissolved in 7.5 M HNO_3. Samples were loaded in 500 μL 3 M HNO_3 onto Sr columns containing 150 μL Eichrom Strontium specific resin bed in 500 μL 3 M HNO_3.

The column was washed and eluted in several stages with HNO_3 following the procedure outlined by (Aciego et al., 2009b). The procedural Sr blank was less than ~60 pg, constituting < 0.1% of the total Sr analyzed for a typical Sr analysis. Strontium samples were loaded onto outgassed 99.98% Re filaments in 1.0 μL 7.5 N HNO_3 along with 0.8 μL TaF_5 activator to enhance the ionization efficiency of Sr (Charlier et al., 2006).

Strontium isotope measurements were performed on a Thermo-Finnigan Triton Plus Thermal Ionization Mass Spectrometer (TIMS) at the University of Michigan using the method outlined in Stevenson et al., (2015b). Fractionation caused during machine analysis was corrected for using $^{86}Sr/^{88}Sr = 0.1194$. External precision on the standard runs (NBS987) for $^{87}Sr/^{86}Sr$ was 0.710264 ± 0.000016 (2 s.d. n=50). A basalt rock (BCR-2) was used to monitor precision of column chemistry and TIMS analysis. The $^{87}Sr/^{86}Sr$ of BCR-2 was within error of literature 0.70504±5 (2 s.d. in the last decimal place, n=3), respectively (e.g. Krabbenhöft et al., 2009; Ma et al., 2013; Moynier et al., 2010).

4. Results

4.1 Physiochemical Properties

The seasonal physiochemical dataset of the LCG and AG can be found in Appendices A and B, respectively. Appendix B additionally contains the diurnal values from August and October cycles at the AG. Greater discharge, alkalinity, and conductivities characterize measurements from the AG in comparison to the LCG. In general, the pH is higher at the AG (average pH = 8.89; 2 s.d. of 0.37) than the LCG (average pH = 7.40; 2 s.d. of 0.40). It is important to highlight that field seasons at the AG and LCG did not occur at the same time of year, with sample for the AG from JD 223—298 and for the LCG from JD 182—252. At the LCG the pH begins to increase starting JD 238 and reached a maximum measured pH on JD 248 whereas sampling at the AG did not begin until JD 223. Daily precipitation trends, provided by the Agroclimatic Information Service (ACIS, 2015) and the NOAA Juneau Airport weather station (NOAA, 2014), are additionally reported in Figure 3 and Figure 4, respectively.

4.2 Radiogenic isotope measurements

Appendices C and D present the seasonal radiogenic Sr and Nd measurements at the LCG and AG, respectively. Errors are reported as two standard errors of the mean and are given in parentheses with variation in the last decimal place. Correlations between the $^{87}Sr/^{86}Sr$ and ε_{Nd} are presented in Figures 5 and 6 for the LCG and AG, respectively, and include both time-series and diurnal values. The plots contrast the wide ε_{Nd} and narrow $^{87}Sr/^{86}Sr_{range}$ at the LCG with the narrow ε_{Nd} range and wide $^{87}Sr/^{86}Sr_{range}$ at the AG.

4.2.1 Radiogenic Neodymium

The time-series Nd isotopic values are recorded in Appendices C and D and depicted in Figure 3 and 4 for the LCG and AG, respectively. The Nd isotopic compositions are represented in epsilon notation as ε_{Nd} (Eq. 1), which is defined as:

$$\varepsilon_{Nd(t)} = \left[\frac{\left(\frac{^{143}Nd}{^{144}Nd}\right)_{sample(t)}}{\left(\frac{^{143}Nd}{^{144}Nd}\right)_{CHUR(t)}} - 1\right] \times 10000$$

(Eq. 1)

where $(^{143}Nd/^{144}Nd)_{CHUR}$ is the Nd isotopic composition of the Chondritic Uniform Reservoir (CHUR) which is $^{143}Nd/^{144}Nd = 0.512638$ (Jacobsen and Wasserburg, 1980).

The internal error of 2σ of the mean is parenthesized for each value and external error is $\varepsilon_{Nd} = 0.49$.

At the LCG, we observe an average radiogenic Nd value of $\varepsilon_{Nd} = -6.2 \pm 1.0$ (2 s.d.). The greatest degree of spread is observed between JD 216 to 234. Values range from ε_{Nd} of -4.6 (0.9) to -8.7 (0.2). The remaining subset from JD 230—251 exhibits an average $\varepsilon_{Nd} = -6.2 \pm 1.1$ (2 s.d.) and mirror early season values.

The time-series AG values are presented in Figure 4. The dataset exhibits little seasonal variability with an average ε_{Nd} of -27.3 ± 0.6 (2 s.d.), which is only slightly larger than the external reproducibility of $\varepsilon_{Nd} = 0.49$. Similarly, the diurnal values reported in Appendix D align with the time-series record. We report averages of ε_{Nd} =-27.5 ± 0.7 and -27.3 ± 0.5 for the August and October cycles, respectively and with two standard deviations.

4.2.2 Radiogenic Strontium

In a corresponding study, Stevenson et al. (In review-a) analyzed the radiogenic Sr isotopic compositions of the suspended sediment from JD 226—252 at the LCG. The LCG dataset exhibits a slightly parabolic seasonal record. The measurements trend towards less radiogenic values from JD 182—213 (R^2= 0.93) with a measured $^{87}Sr/^{86}Sr_{range}$ = 0.709673(8) to 0.708562(8). Mid-season values from JD 214—235 exhibit poor correlation ($R^2 = 0.06$), coinciding the mid-season spread of measured ε_{Nd} values. During the time-period, we report an average value of 0.709054 ± 0.00352 (2 s.d.). At the end of the season (JD 236—251), increases towards more radiogenic values mark seasonal progression ($^{87}Sr/^{86}Sr$ = 0.709036(6) to 0.70975(1); $R^2 = 0.20$).

The time-series radiogenic Sr values from the AG (Figure 4) exhibit higher isotopic ratios, which generally decrease over the course of the melt season ($^{87}Sr/^{86}Sr_{range}$ of 0.712424(7) to 0.71606(2); $R^2 = 0.34$); however, the correlation is stronger at the beginning of the melt season (JD 233-267; $R^2 = 0.45$). A greater range of seasonal variability is observed at the AG than the LCG ($^{87}Sr/^{86}Sr_{range} = 0.0036$ versus 0.0015, respectively).

Total variation in $^{87}Sr/^{86}Sr_{range}$ over a diurnal cycle are much larger for August, 0.0014, compared to October 0.0004. While no discernable trend exists in the October record, there is a shift towards less radiogenic values from 10:00 to 20:00, which is followed by an increase in the isotopic ratio from 20:00 to 4:00. However, consistently high discharge measurements occurred during the August diurnal sampling with all values greater than 0.75 $m^3\ s^{-1}$. The observed trends from the diurnal and time-series samples correlate well to in-situ discharge measurements (Figure 7). The $^{87}Sr/^{86}Sr$ ratio increases with discharge ($R^2 = 0.52$) until a critical value of 0.9 $m^3\ s^{-1}$ was reached. High variability in the $^{87}Sr/^{86}Sr$ ratio is apparent at high discharge levels during both diurnal and time-series measurements.

4.3 Elemental Concentrations

Elemental concentrations from the AG are reported in Appendix B. In general, Al, Ca, K, Mg, Na, Rb, seasonal trends are highly variable, with peaks on JD 243, 244, and 290. Rain events did occur on each of these days; however, there are no consistent seasonal trends between the daily elemental variation and the rain events or total discharge. While individual concentrations indicate mineralogical variability of the sediment, molar ratios track seasonal weathering trends. Here, we refer to the Rb/Sr, Sm/Nd, and Ca/K values listed in Appendix B. A strong, positive correlation between the $^{87}Sr/^{86}Sr$ and Rb/Sr ratios for the time-series dataset ($R^2 = 0.79$) (Figure 8) encapsulates the traditional Rb-Sr isochron. Inclusion of the diurnal ratios weakens the trend ($R^2 = 0.57$), particularly as the October cycle exhibits relatively high Rb/Sr ratios and low $^{87}Sr/^{86}Sr$ values. A moderate, inverse relationship exists between the $^{87}Sr/^{86}Sr$ and Ca/K ratios (Figure 9, $R^2 = 0.47$ for the entire dataset). However, there is no correlation between ε_{Nd} and the seasonal Ca/K, further emphasizing the lack of variability in the ε_{Nd} record.

Due to the limited variability in the ε_{Nd} ratios, we examined variation in Nd concentrations though the Sm/Nd ratio as a comparative plot to Figure 8. There is weak, positive trend ($R^2 = 0.17$) between the Sm/Nd and total discharge over the entire dataset (Figure 11, in the Supplementary Online Material). The August diurnal values exhibit a distinctly wide range of Sm/Nd which correlate with high discharge volumes consistently greater than 2.7 $m^3 s^{-1}$ and captures peak melt conditions that occur at approximately 16:00. Still, exclusion of the diurnal cycles leads to a weak correlation ($R^2 = 0.09$).

5. Discussion

5.1 Characterizing the subglacial environment utilizing combined Sr-Nd analysis

Combining radiogenic Nd and Sr isotopic systems has greatly enhanced the current understanding of how sediment is sourced (Goldstein and Jacobsen, 1988; McCulloch et al., 2003; Yang et al., 2007), transported (Viers et al., 2008; Weldeab et al., 2002), and weathered (Lupker et al., 2013; Négrel, 2006) in rivers and soils. Our case studies present two contrasting scenarios regarding the processing and mixing of sediment in the subglacial environment. Differences between the systems help us to classify sediment transport mechanisms into two distinct categories: poorly-mixed and well-mixed subglacial suspended sediment.

5.1.1 Poorly mixed suspended sediment

The LCG exhibits a wide range of ε_{Nd} values, ($\varepsilon_{Nd\ (Range)}$ = 4.1). In rare instances, intense weathering of basalts has been attributed to ε_{Nd} drifts of ~2.5 (Ma et al., 2010), which is still notably lower than the LCG variability. The few studies reporting annual variability of the dissolved and suspended sediment loads in global rivers has been within the range of $\varepsilon_{Nd\ (Range)}$ = 1-2.5 (e.g. Andersson et al., 2001; Viers et al., 2008). However, a large variability has been reported in suspended sediments within the major channel and tributaries along the Yangtze River ($\varepsilon_{Nd\ (Range)}$ = 3.9), which has been attributed to lack of dominant source rocks and complicated underlain geology ranging from Archean to Quaternary material (Yang et al., 2007).

While the geology beneath the LCG is primarily mid-Cretaceous, late-Permian facies extend to the west and underlay part of the glacial head. Geologic units underlying the LCG also include: biotite schist, biotite gneiss, marble and calc-silicate granofels, hornblende gneiss, and granitoid rocks (Brew and Ford, 1985). In comparison, the AG is predominately underlain by Middle Cambrian shales and limestones. These differences may create a hydrologic environment where there exists a greater variation in sediment age and composition at the LCG.

While the individual glaciers (LCG and AG) are relatively similar in length (Hart, 2006; Miller and Pelto, 1999), the differences in range of the isotopic values may be a consequence of the rate of discharge levels or environmental forcings within the subglacial system. At lower discharge rates, there may be a greater potential for heterogeneities (e.g. previously isolated cavities containing sediment pockets) to impact the bulk measured sediment ratio at the terminus of the glacier (sample site). This is because the sample is only a snapshot of the inferred daily sediment load. As discharge increases, greater flow levels could provide enough peak shear stress for more consistent and well-mixed excavations. Still, the alternative explanative of an environmental forcing to the system is more compelling.

At the LCG, the greatest spread in ε_{Nd} values occurs within JD 216—234, during which the drainage network has likely reached its full extent. The subsequent range narrows and aligns with early season values; the excluded subset exhibits an average ε_{Nd} value of -6.2 ± 1.0 (2 s.d.). This period of high variability also coincides with the drainage of periglacial Lake Linda, which is located at the head of the glacier. Each summer, rapid drainage events cause the water to flow throughout the glacier. Complete drainage has been observed to occur over a 48-hour period and the event may occur on separate times during the summer. In 2012, a flyover on JD 213 affirmed the lake had not yet drained. However, a sampling excursion on JD 230 revealed that drainage had occurred. During the drainage, the abrupt flux of water may have overwhelmed the system and mobilized the surface texture, which may have freed interlocked or underlain grains. Such disturbances could also maximize the introduction of unexposed sediment pockets. As the season progressed past JD 234, the transport network may then have reequilibrated. However, we see little evidence of a change in measured discharge during this period that would have been expected with the abrupt Lake Linda drainage. This may further emphasize the uncertainty that can be associated with subglacial dynamics.

Precipitation may play a qualifying role as well. There was a higher frequency of precipitation across the sample collection period at the LCG than the AG (Figure 3 *vs*. Figure 4). As water transported from the surface and through englacial conduits plays an important role in the total water flux, consistent perturbations could cause the subglacial regime to shift and evolve on a small scale. While no consistent trend between precipitation and isotopic ratios exists, there may potentially be lead-lag relations. Hence, when using fluvial sediment as a source provenance, it may be important to assess potential disruptions to the hydrologic network as they may amplify heterogeneity and obscure chemical weathering signals. Suspended sediment itself can be more heterogeneous in mineralogy than dissolved sediment in nature. The composition of the dissolved load relates more to which minerals are preferentially dissolved through chemical alteration whereas the composition of the suspended load relates to the eroded residue, secondary mineral phases, and the introduction of additional authigenic minerals (Tricca et al., 1999). Further comparison between the subglacial environments from different climatic regimes could elucidate our understanding of the impact of climatic events on the partitioning of chemical signatures between the dissolved and suspended sediment loads.

5.1.2 Well-mixed suspended sediment

In contrast to the LCG, limited variability is observed in the Sr-Nd record at the AG. The consistency does not oversimplify the depositional processes within the subglacial environment. Rather, it suggests a continuous, dynamic manner in which the sediment is mixed. The result is a similarly aged product, as reflected in the ε_{Nd} values. The overall greater flow-through discharge measurements may reflect greater entrainment and transport of available sediment. Comparison between the LCG and AG bedrock suggests shifts in the ε_{Nd} record would be observed at both sites. The rotation of the bedrock during the genesis of the Canadian Rockies leads to a general in decrease in bedrock age in the northeast direction, or down-glacier (Figure 2). One explanation is also that the age-gradient could be insignificant on the scale of the AG. An undetermined variable however is that samples from the AG were collected later in the melt season than the LCG (JD 223-298 versus JD 189-252, respectively). Despite potential complications of drainage evolution and progressive closure of basal network, the values remain constant through the end of the season. This measurement consistency proves interesting as it enables us to unravel incongruent weathering trends in the radiogenic Sr record.

5.2 Strontium weathering signal and depositional implications

The AG isotopic record requires additional attention due to its insignificant variation in the ε_{Nd} ratios over the course of the melt season and large scale of variability in the $^{87}Sr/^{86}Sr$ record (approximately twice the observed radiogenic Sr variability at the LCG). The dual combination promotes observation of chemical weathering trends as variation due to bedrock source changes has been eliminated. Négrel (2006) has related similar trends to incongruent weathering mechanisms in soils and waters. Hence, it is important to analyze the Sr systematics with their corresponding elemental data to determine if the comparisons between traditional, well-studied weathering environments and the subglacial environment can be systematic.

The $^{87}Sr/^{86}Sr$ against the Rb/Sr ratio is presented in Figure 8. While the measured trends follow traditional isochron lines (Goldstein and Jacobsen, 1988), the AG plot does not represent variation in geologic age and instead likely represents a mineralogical control on the radiogenic Sr composition of the sediments (Colin et al., 2006; Singh and France-Lanord, 2002). Small deviations create a slightly sub-linear array. Brass (1975) attributed partial causation to the retention of Rb during weathering of sediments and preferential leaching of Sr. Slight complications may also occur due to the presence of un-metamorphosed sedimentary rocks (Eisenhauer et al., 1999), and studies generally present greater scatter in suspended sediment than dissolved sediment trends (Goldstein and Jacobsen, 1988).

To further support the weathering model, Figure 9 reveals an inverse relationship between the $^{87}Sr/^{86}Sr$ ratios and the Ca/K ratio. Carbonate minerals within the bedrock are preferentially dissolved during weathering in the subglacial environment (e.g. Fairchild et al., 1994; Tranter et al., 1993) and the plot reinforces the release of low $^{87}Sr/^{86}Sr$ bearing minerals during the initial stages of chemical weathering followed by the release of more radiogenic $^{87}Sr/^{86}Sr$ K-bearing minerals during slower, silicate weathering. The relationship combines with this pseudo-isochron to provide the conceptual framework for detecting chemical weathering trends through correlation of radiogenic Sr record and hydrologic parameters.

Comminution through physical weathering processes leads to the exposure of fresh, reactive surfaces. While these reactive surfaces may be primed for chemical alteration, glacierized environments have been generally reported to have relatively higher physical and lower chemical weathering rates in comparison to non-glacierized environment due to high levels of glacial erosion and abrasion (Raiswell et al., 2006). The ratio of the two weathering rates may contribute unique characteristics to sediments produced in the subglacial environment. In particular, the time elapsed since initial comminution, and hence sediment formation, has taken place may help explain trends between the $^{87}Sr/^{86}Sr$ ratios and hydro-physical properties such as bulk discharge (Figure 7). While the geologic age of the sediment presents as invariable, we suggest the concept of a post-comminution age to describe the correlation and depositional processes.

Subglacial deposition may simply be a function of the net sediment flux into a given subglacial area (Hart, 1995) whereas entrainment occurs when a critical shear stress at the bed is exceeded (Walder and Fowler, 1994). The texture of the subglacial environment is largely unconstrained; however, the AG does maintain a layer of deformable subglacial till (Hart, 2006). Subglacial diamict is highly variable in grain size (e.g. Drewry, 1986) and has been described to maintain a matrix rich in clay and silt-sized grains, presumably derived from comminution processes (Walder and Fowler, 1994). Excavation of sediment is thought to differ between such soft beds and contrasting rigid beds (longitudinal movement of sediment at the base of deforming layer *vs*. erosion by plucking and abrasion, respectively) (Hart, 1995), and thus we would expect excavation at the AG to be dependent on the depositional layering of sediment.

There is an increase in $^{87}Sr/^{86}Sr$ ratios until a seemingly critical discharge value of ~0.9 $m^3 s^{-1}$ is reached at the AG. Critical discharges are likely unique to a given glacier and may depend on the location, bed topography, and climatic factors. The relationship suggests that, as flow rates increase, sediment with a younger post-comminution age will become entrained. As the mantle is deepened, as shown in Figure 10, 'older' sediment is exposed and primed for transport. However, once the critical discharge is reached, excavation of sediment is likely non-discriminatory, which may be due shear stresses exceeding conditions for equal mobility or the additional inclusion of previously isolated sediment. All available sediment has the same potential to flush out of the system. The consistency of this trend has implications for the production of sediment throughout the melt season. Often, the greatest sediment loads are excavated at the beginning of the melt season due to the build-up of sediment during the low flow and likely less channelized drainage network during the winter months (e.g. Collins, 1990). Our field campaign occurred during the final stage of the melt season (August—October), which suggests the depositional environment continues to evolve on a daily scale throughout the entire melt season.

The results pose the unanswered question of the impact of a soft, deformable layer. If quarrying effects are only observed concurrently with similar soft-sediment layers, they may be requisite. Unfortunately, comparative analysis from the LCG is inconclusive due to the high variation of ε_{Nd} record.

5.3 Diurnal Variability at the Athabasca Glacier

The diurnal AG isotopic and elemental trends are relatively consistent with the time-series values. The sampling in August indicates high discharge levels (> 0.7 $m^3 s^{-1}$) throughout the day with peak discharge levels occurring in the afternoon. The resulting high $^{87}Sr/^{86}Sr_{range}$ further supports the importance of flow conditions to the understanding of sediment transport, entrainment, and erosion. While it is expected that heterogeneities are inherent to chemical characterization of sediment, our study suggests the presence of systemic depositional processes (e.g. mantling) exist on short temporal scales. The October sampling aligns with a majority of the time-series trends (Figure 6, 7, and 9). However, the $^{87}Sr/^{86}Sr$ *vs*. Rb/Sr molar ratio exhibits a distinctly low $^{87}Sr/^{86}Sr$ for given Rb/Sr values (Figure 8). As the October sampling likely occurred during the progressive closure of the drainage network, an increase of preferential leaching of mobile Sr may help explain these observations.

6. Conclusions

High physical weathering rates within the subglacial drainage network could largely impact how the suspended sediment is processed, deposited, and entrained. In an attempt to reveal subglacial dynamics, our study presents the first application of Sr-Nd systematics to the suspended sediment of the subglacial meltwater. The systematics traditionally track variation of source and weathering in fluvial environments. The Sr-Nd correlation reported in our study provides important implications for how well the sediment is mixed as it is processed through the drainage network at two geologically distinct glaciers.

Time-series values at the LCG that show high variability in the ε_{Nd} values suggest a poorly mixed sediment flux. The variation may relate to a glacial flood event, which suggests the sediment transport is sensitive to local climate disturbances. Such events may lead to a period of disequilibrium within the depositional environment and the implications suggest degree of caution should be taken when assessing weathering trends. Conversely, the insights gained from records of low seasonal variability in the ε_{Nd} record strengthens our ability to understand chemical and physical processes affecting the radiogenic Sr record. At the AG, correlation between the $^{87}Sr/^{86}Sr$ ratios and total discharge measurements suggest the occurrence of bedrock mantling. We track the process through the post-comminution age of the suspended sediment for which we capitalize on traditional radiogenic Sr systematics to construct a pseudo-isochron of the suspended sediment. Such depositional characteristic may be unique to glaciers with soft, deformable beds. Application to additional subglacial environments with diverse geology, subglacial texture, and locations would provide useful comparisons for future analysis. The introduction of more isotopic tracers such as lead or hafnium could constrain our interpretation further. As we continue to geochemically characterize the processes affecting the erosion, deposition, and transport of the subglacial sediment, a greater quantification of how the subglacial sediment flux impacts the underlying depositional environment and downstream ecosystems may be facilitated.

Acknowledgements

Funding was provided by the Department of Earth & Environmental Sciences Turner Award and the Geological Society of America undergraduate research grant to

AEC and by the Packard Foundation to SMA. Thank you to Ted Houston for trace element analysis, Molly Blakowski, Yi-Wei Lui, Kyle Meyer, and Walt Afonso for field assistance, and University of Michigan Undergraduate Research Opportunity Program students Megan Wiltse, Nickolas Adamowicz, and Rohan Mehta for laboratory assistance.

References

Aarons, S.M., Aciego, S., Gleason, J., 2013. Variable Hf Sr Nd radiogenic isotopic compositions in a Saharan dust storm over the Atlantic: Implications for dust flux to oceans, ice sheets and the terrestrial biosphere. Chemical Geology, 349, 18-26.

Aciego, S., Stevenson, E., Arendt, C., 2015. Climate versus geological controls on glacial meltwater micronutrient production in southern Greenland. Earth and Planetary Science Letters, 424, 51-58.

Aciego, S.M., Bourdon, B., Lupker, M., Rickli, J., 2009a. A new procedure for separating and measuring radiogenic isotopes (U, Th, Pa, Ra, Sr, Nd, Hf) in ice cores. Chemical Geology, 266(3), 194-204.

Aciego, S.M., Bourdon, B., Lupker, M., Rickli, J., 2009b. A new procedure for separating and measuring radiogenic isotopes (U, Th, Pa, Ra, Sr, Nd, Hf) in ice cores. Chem Geol, 266(3-4), 194-204.

ACIS, 2015. Agroclimatic Information Service (ACIS). In: A.A.a.R. Development (Ed.).

Allègre, C.J., Louvat, P., Gaillardet, J., Meynadier, L., Rad, S., Capmas, F., 2010. The fundamental role of island arc weathering in the oceanic Sr isotope budget. Earth and Planetary Science Letters, 292(1), 51-56.

Alley, R.B., Cuffey, K.M., Evenson, E.B., Strasser, J.C., Lawson, D.E., Larson, G.J., 1997. How glaciers entrain and transport basal sediment: Physical constraints. Quaternary Science Reviews, 16(9), 1017-1038.

Anderson, R.S., Anderson, S.P., MacGregor, K.R., Waddington, E.D., O'Neel, S., Riihimaki, C.A., Loso, M.G., 2004. Strong feedbacks between hydrology and sliding of a small alpine glacier. Journal of Geophysical Research, 109(F3).

Anderson, S.P., 2007. Biogeochemistry of glacial landscape systems. Annual Review of Earth and Planetary Sciences, 35, 375-399.

Andersson, P.S., Dahlqvist, R., Ingri, J., Gustafsson, Ö., 2001. The isotopic composition of Nd in a boreal river: a reflection of selective weathering and colloidal transport. Geochimica et Cosmochimica Acta, 65(4), 521-527.

Archive, C.N.C., 2013. Canada National Climate Archive, Natl. Clim. Data Cent. National climate data and information archive technical report no. Alberta 5, 2011-7, 2011, Fredericton, New Brunswick, Canada.

Arendt, C.A., Aciego, S.M., Hetland, E.A., 2015. An open source Bayesian Monte Carlo isotope mixing model with applications in Earth surface processes. Geochemistry, Geophysics, Geosystems.

Arendt, C.A., Aciego, S.M., Sims, K.W., Robbins, M., 2014. Sequential Separation of Uranium, Hafnium and Neodymium from Natural Waters Concentrated by Iron Coprecipitation. Geostandards and Geoanalytical Research.

Arn, K., Hosein, R., Föllmi, K.B., 2003. Strontium isotope systematics in two glaciated crystalline catchments: Rhone and Oberaar Glaciers (Swiss Alps). Schweizerische mineralogische und petrographische Mitteilungen, 83, 273-283.

Bain, D., Bacon, J., 1994. Strontium isotopes as indicators of mineral weathering in catchments. Catena, 22(3), 201-214.

Bingham, R.G., Nienow, P.W., Sharp, M.J., Boon, S., 2005. Subglacial drainage processes at a High Arctic polythermal valley glacier. Journal of Glaciology, 51(172), 15-24.

Blum, J.D., Erel, Y., 1995. A Silicate Weathering Mechanism Linking Increases in Marine Sr-87/Sr-86 with Global Glaciation. Nature, 373(6513), 415-418.

Blum, J.D., Erel, Y., Brown, K., 1993. Sr-87/Sr-86 Ratios of Sierra-Nevada Stream Waters - Implications for Relative Mineral Weathering Rates. Geochim Cosmochim Ac, 57(21-22), 5019-5025.

Boghossian, N.D., Patchett, P.J., Ross, G.M., Gehrels, G.E., 1996. Nd isotopes and the source of sediments in the miogeocline of the Canadian Cordillera. The Journal of Geology, 259-277.

Boulton, G., Dobbie, K., Zatsepin, S., 2001. Sediment deformation beneath glaciers and its coupling to the subglacial hydraulic system. Quaternary International, 86(1), 3-28.

Brass, G.W., 1975. The effect of weathering on the distribution of strontium isotopes in weathering profiles. Geochimica et Cosmochimica Acta, 39(12), 1647-1653.

Brew, D.A., Ford, A.B., 1985. Preliminary reconnaissance geologic map of the Juneau, Taku River, Atlin, and part of the Skagway 1: 250,000 quadrangles, southeastern Alaska. 2331-1258, US Geological Survey.

Brown, G.H., 2002. Glacier meltwater hydrochemistry. Applied Geochemistry, 17(7), 855-883.

Brown, G.H., Tranter, M., Sharp, M., 1996. Experimental investigations of the weathering of suspended sediment by alpine glacial meltwater. Hydrological Processes, 10(4), 579-597.

Capo, R.C., Stewart, B.W., Chadwick, O.A., 1998. Strontium isotopes as tracers of ecosystem processes: theory and methods. Geoderma, 82(1–3), 197-225.

Charlesworth, H., Erdmer, P., 1989. Geology of the Rocky Mountains between the Athabasca and North Saskatchewan Rivers, Edmonton Geological Society.

Charlier, B.L.A., Ginibre, C., Morgan, D., Nowell, G.M., Pearson, D.G., Davidson, J.P., Ottley, C.J., 2006. Methods for the microsampling and high-precision analysis of strontium and rubidium isotopes at single crystal scale for petrological and geochronological applications. Chemical Geology, 232(3-4), 114-133.

Clow, D.W., Mast, M.A., Bullen, T.D., Turk, J.T., 1997a. Strontium 87 strontium 86 as a tracer of mineral weathering reactions and calcium sources in an alpine/subalpine watershed, Loch Vale, Colorado. Water Resour Res, 33(6), 1335-1351.

Clow, D.W., Mast, M.A., Bullen, T.D., Turk, J.T., 1997b. Strontium 87/strontium 86 as a tracer of mineral weathering reactions and calcium sources in an alpine/subalpine watershed, Loch Vale, Colorado. Water Resources Research, 33(6), 1335-1351.

Colin, C., Turpin, L., Blamart, D., Frank, N., Kissel, C., Duchamp, S., 2006. Evolution of weathering patterns in the Indo‐Burman Ranges over the last 280 kyr: Effects of sediment provenance on 87Sr/86Sr ratios tracer. Geochemistry, Geophysics, Geosystems, 7(3).

Collins, D.N., 1988. Seasonal development of subglacial drainage and suspended sediment delivery to meltwaters beneath an Alpine glacier. Department of Geography, University of Manchester.

Collins, D.N., 1990. Seasonal and annual variations of suspended sediment transport in meltwaters draining from an Alpine glacier. Hydrology in Mountainous Regions I: Hydrological Measurements; the Water Cycle, 439-446.

Derry, L.A., France-Lanord, C., 1996. Neogene Himalayan weathering history and river 87Sr/86Sr: impact on the marine Sr record. Earth and Planetary Science Letters, 142(1), 59-74.

Drewry, D., 1986. Glacial geologic processes. Edward Arnold Baltimore.

Edmond, J., 1992. Himalayan tectonics, weathering processes, and the strontium isotope record in marine limestones. Science, 258(5088), 1594-1597.

Eisenhauer, A., Meyer, H., Rachold, V., Tütken, T., Wiegand, B., Hansen, B., Spielhagen, R., Lindemann, F., Kassens, H., 1999. Grain size separation and sediment mixing in Arctic Ocean sediments: evidence from the strontium isotope systematic. Chemical Geology, 158(3), 173-188.

Evans, D., Phillips, E., Hiemstra, J., Auton, C., 2006. Subglacial till: formation, sedimentary characteristics and classification. Earth-Science Reviews, 78(1), 115-176.

Fairchild, I.J., Bradby, L., Sharp, M., Tison, J.-L., 1994. Hydrochemistry of carbonate terrains in alpine glacial settings. Earth Surface Processes Landforms, 19, 33-54.

Fountain, A.G., Walder, J.S., 1998. Water flow through temperate glacier. Rev. Geophys., 36(3), 299-328.

Fujita, K., 2008. Effect of precipitation seasonality on climatic sensitivity of glacier mass balance. Earth and Planetary Science Letters, 276(1), 14-19.

Garçon, M., Chauvel, C., France-Lanord, C., Limonta, M., Garzanti, E., 2014. Which minerals control the Nd–Hf–Sr–Pb isotopic compositions of river sediments? Chemical Geology, 364, 42-55.

Gehrels, G., Brew, D., Saleeby, J., 1984. Progress report on U/Pb (zircon) geochronologic studies in the Coast plutonic-metamorphic complex east of

Juneau, southeastern Alaska. This publication is part of a larger work. Please see C-939 for more information. Department of Natural Resources, Division of Geological & Geophysical Surveys (DGGS) 3354 College Road, Fairbanks, AK .

Goldstein, S.J., Jacobsen, S.B., 1988. Nd and Sr isotopic systematics of river water suspended material: implications for crustal evolution. Earth and Planetary Science Letters, 87(3), 249-265.

Hart, J.K., 1995. Subglacial erosion, deposition and deformation associated with deformable beds. Progress in Physical Geography, 19(2), 173-191.

Hart, J.K., 2006. Athabasca Glacier, Canada–a field example of subglacial ice and till erosion? Earth Surface Processes and Landforms, 31(1), 65-80.

Hedin, R.S., Watzlaf, G.R., Nairn, R.W., 1994. Passive treatment of acid mine drainage with limestone. Journal of Environmental Quality, 23(6), 1338-1345.

Hindshaw, R.S., Rickli, J., Leuthold, J., Wadham, J., Bourdon, B., 2014. Identifying weathering sources and processes in an outlet glacier of the Greenland Ice Sheet using Ca and Sr isotope ratios. Geochimica et Cosmochimica Acta, 145, 50-71.

Hodge, S.M., 1976. Direct measurement of basal water pressures: a pilot study. Journal of Glaciology, 16, 205-218.

Hodgkins, R., Tranter, M., Dowdeswell, J., 1995. The interpretation of hydrochemical evidence for meltwater routing at a high Arctic glacier. IAHS Publications-Series of Proceedings and Reports-Intern Assoc Hydrological Sciences, 228, 387-394.

IPCC, 2013. Climate Change 2013: The Physical Science Basis: Working Group I Contribution to the Fifth Assessment Report of the Intergovernment Panel on Climate Change. Cambridge University Press, Cambridge.

Jacobsen, D., Milner, A.M., Brown, L.E., Dangles, O., 2012. Biodiversity under threat in glacier-fed river systems. Nature Climate Change, 2(5), 361-364.

Jacobsen, S.B., Wasserburg, G., 1980. Sm-Nd isotopic evolution of chondrites. Earth and Planetary Science Letters, 50(1), 139-155.

Jiang, F., Frank, M., Li, T., Xu, Z., Li, A., 2013. Asian dust input in the western Philippine Sea: Evidence from radiogenic Sr and Nd isotopes. Geochemistry, Geophysics, Geosystems, 14(5), 1538-1551.

Jones, C.E., Halliday, A.N., Rea, D.K., Owen, R.M., 1994. Neodymium isotopic variations in North Pacific modern silicate sediment and the insignificance of detrital REE contributions to seawater. Earth and Planetary Science Letters, 127(1–4), 55-66.

Kistler, R.W., Newberry, R.J., Brew, D.A., 1993. Vein minerals in the Juneau Gold Belt, Alaska. Geologic Studies in Alaska by the US Geological Survey, 1992, 236.

Kite, G., Reid, I., 1977. Volumetric change of the Athabasca Glacier over the last 100 years. Journal of Hydrology, 32(3), 279-294.

Krabbenhöft, A., Fietzke, J., Eisenhauer, A., Liebetrau, V., Bohm, F., Vollstaedt, H., 2009. Determination of radiogenic and stable strontium isotope ratios ((87)Sr/(86)Sr; delta(88/86)Sr) by thermal ionization mass spectrometry applying an (87)Sr/(84)Sr double spike. J Anal Atom Spectrom, 24(9), 1267-1271.

Krishnaswami, S., Trivedi, J.R., Sarin, M.M., Ramesh, R., Sharma, K.K., 1992. Strontium isotopes and rubidium in the Ganga-Brahmaputra river system: Weathering in the Himalaya, fluxes to the Bay of Bengal and contributions to the evolution of oceanic87Sr/86Sr. Earth and Planetary Science Letters, 109(1–2), 243-253.

Lamb, H., Tranter, M., Brown, G., Hubbard, B., Sharp, M., Gordon, S., Smart, C., Willis, I., Nielsen, M., 1995. The composition of subglacial meltwaters sampled from boreholes at the Haut Glacier d'Arolla, Switzerland. IAHS Publications-Series of Proceedings and Reports-Intern Assoc Hydrological Sciences, 228, 395-404.

Lawson, D.E., 1993. Glaciohydrologic and glaciohydraulic effects on runoff and sediment yield in glacierized basins, DTIC Document.

Li, C.-F., Chen, F., Li, X.-H., 2007. Precise isotopic measurements of sub-nanogram Nd of standard reference material by thermal ionization mass spectrometry using the NdO+ technique. International Journal of Mass Spectrometry, 266(1), 34-41.

Lupker, M., France-Lanord, C., Galy, V., Lavé, J., Kudrass, H., 2013. Increasing chemical weathering in the Himalayan system since the Last Glacial Maximum. Earth and Planetary Science Letters, 365, 243-252.

Ma, J., Wei, G., Xu, Y., Long, W., 2010. Variations of Sr–Nd–Hf isotopic systematics in basalt during intensive weathering. Chemical Geology, 269(3–4), 376-385.

Ma, J.L., Wei, G.J., Liu, Y., Ren, Z.Y., Xu, Y.G., Yang, Y.H., 2013. Precise measurement of stable (delta Sr-88/86) and radiogenic (Sr-87/Sr-86) strontium isotope ratios in geological standard reference materials using MC-ICP-MS. Chinese Sci Bull, 58(25), 3111-3118.

McCulloch, M., Pailles, C., Moody, P., Martin, C.E., 2003. Tracing the source of sediment and phosphorus into the Great Barrier Reef lagoon. Earth and Planetary Science Letters, 210(1), 249-258.

Miller, M.M., Pelto, M.S., 1999. Mass balance measurements on the Lemon Creek Glacier, Juneau Icefield, Alaska 1953–1998. Geografiska Annaler: Series A, Physical Geography, 81(4), 671-681.

Millot, R., érôme Gaillardet, J., Dupré, B., Allègre, C.J., 2003. Northern latitude chemical weathering rates: clues from the Mackenzie River Basin, Canada. Geochimica et Cosmochimica Acta, 67(7), 1305-1329.

Milner, A.M., Brown, L.E., Hannah, D.M., 2009. Hydroecological response of river systems to shrinking glaciers. Hydrological Processes, 23(1), 62-77.

Moore, P.L., Winberry, J.P., Iverson, N.R., Christianson, K.A., Anandakrishnan, S., Jackson, M., Mathison, M.E., Cohen, D., 2013. Glacier slip and seismicity induced by surface melt. Geology, 41(12), 1247-1250.

Moynier, F., Agranier, A., Hezel, D.C., Bouvier, A., 2010. Sr stable isotope composition of Earth, the Moon, Mars, Vesta and meteorites. Earth Planet Sc Lett, 300(3-4), 359-366.

Muhlfeld, C.C., Giersch, J.J., Hauer, F.R., Pederson, G.T., Luikart, G., Peterson, D.P., Downs, C.C., Fagre, D.B., 2011. Climate change links fate of glaciers and an endemic alpine invertebrate. Climatic Change, 106(2), 337-345.

Négrel, P., 2006. Water–granite interaction: clues from strontium, neodymium and rare earth elements in soil and waters. Applied Geochemistry, 21(8), 1432-1454.

Nienow, P., Sharp, M., Willis, I., 1998. Seasonal changes in the morphology of the subglacial drainage system, Haut Glacier d'Arolla, Switzerland. Earth Surface Processes and Landforms, 23(9), 825-843.

NOAA, 2014. Quality Controlled Local Climatological Data (QCLCD 2.5.5). In: N.-E.P.S. Division (Ed.), Boulder, Colorado.

Öhlander, B., Land, M., Ingri, J., Widerlund, A., 2014. Mobility and Transport of Nd Isotopes in the Vadose Zone during Weathering of Granitic Till in a Boreal Forest. Aquatic Geochemistry, 20(1), 1-17.

Paterson, W., 1964. Variations in velocity of Athabasca Glacier with time. Journal of Glaciology, 5, 277-285.

Paterson, W., Savage, J., 1963. Geometry and movement of the Athabasca Glacier. Journal of Geophysical Research, 68(15), 4513-4520.

Peucker-Ehrenbrink, B., Blum, J.D., 1998. Re-Os isotope systematics and weathering of Precambrian crustal rocks: implications for the marine osmium isotope record. Geochimica et Cosmochimica Acta, 62(19–20), 3193-3203.

Piepgras, D.J., Jacobsen, S.B., 1988. The isotopic composition of neodymium in the North Pacific. Geochimica et Cosmochimica Acta, 52(6), 1373-1381.

Raczek, I., Jochum, K.P., Hofmann, A.W., 2003. Neodymium and Strontium Isotope Data for USGS Reference Materials BCR‐1, BCR‐2, BHVO‐1, BHVO‐2, AGV‐1, AGV‐2, GSP‐1, GSP‐2 and Eight MPI‐DING Reference Glasses. Geostandards Newsletter, 27(2), 173-179.

Raiswell, R., Tranter, M., Benning, L.G., Siegert, M., De'ath, R., Huybrechts, P., Payne, T., 2006. Contributions from glacially derived sediment to the global iron (oxyhydr) oxide cycle: implications for iron delivery to the oceans. Geochimica et Cosmochimica Acta, 70(11), 2765-2780.

Raymond, C.F., 1969. Flow in a transverse section of Athabasca Glacier, Alberta, Canada, California Institute of Technology.

Raymond, C.F., Benedict, R.J., Harrison, W.D., Echelmeyer, K.A., Sturm, M., 1995. Hydrological discharges and motion of Fels and Black-Rapids Glaciers, Alaska, USA - Implications for the structure of their drainage systems. Journal of Glaciology, 41(138), 290-304.

Samson, S.D., Patchett, P.J., McCleeland, W.C., Gehrels, G.E., 1991. Nd isotopic characterization of metamorphic rocks in the Coast Mountains, Alaskan and Canadian Cordillera: ancient crust bounded by juvenile terranes. Tectonics, 10(4), 770-780.

Shea, J.M., Marshall, S.J., 2007. Atmospheric flow indices, regional climate, and glacier mass balance in the Canadian Rocky Mountains. International journal of climatology, 27(2), 233-247.

Sheik, C.S., Stevenson, E.I., Den Uyl, P.A., Arendt, C.A., Aciego, S.M., Dick, G.J., 2015. Microbial communities of the Lemon Creek Glacier show subtle structural variation yet stable phylogenetic composition over space and time. Frontiers in Microbiology, 6, 495.

Singh, S.K., France-Lanord, C., 2002. Tracing the distribution of erosion in the Brahmaputra watershed from isotopic compositions of stream sediments. Earth and Planetary Science Letters, 202(3–4), 645-662.

Stenborg, T., 1969. Studies of the internal drainage of glaciers. Geografiska Annaler. Series A. Physical Geography, 13-41.

Stevenson, E.I., Aciego, S.M., Burton, K.W., Parkinson, I.J., Blakowski, M.A., Arendt, C.A., In review-a. Insights into combined radiogenic and stable strontium isotopes as tracers for weathering processes in subglacial environments. Chemical Geology.

Stevenson, E.I., Aciego, S.M., Liu, Y.-W., Arendt, C.A., In review-b. Glacial catchment seasonal snow and ice melt impacts on the hydrochemistry of the proglacial environment: evidence from the Lemon Creek. Arctic, Antarctic, and Alpine Research, In review.

Swift, D.A., Nienow, P.W., Spedding, N., Hoey, T.B., 2002. Geomorphic implications of subglacial drainage configuration: rates of basal sediment evacuation controlled by seasonal drainage system evolution. Sedimentary Geology, 149(1), 5-19.

Taylor, A., Blum, J.D., 1995. Relation between Soil Age and Silicate Weathering Rates Determined from the Chemical Evolution of a Glacial Chronosequence. Geology, 23(11), 979-982.

Taylor, S.R., McLennan, S.M., 1995. The geochemical evolution of the continental crust. Reviews of Geophysics, 33(2), 241.

Tranter, M., 2003. Geochemical weathering in glacial and proglacial environments. Treatise on geochemistry, 5, 189-205.

Tranter, M., 2005. Geochemical weathering in glacial and proglacial environments. Surface and Groundwater, Weathering and Soils, 5, 189-205.

Tranter, M., Brown, G., Raiswell, R., Sharp, M., Gurnell, A., 1993. A conceptual-model of solute acquisition by alpine glacial meltwaters. Journal of Glaciology, 39(133), 573-581.

Tricca, A., Stille, P., Steinmann, M., Kiefel, B., Samuel, J., Eikenberg, J., 1999. Rare earth elements and Sr and Nd isotopic compositions of dissolved and suspended loads from small river systems in the Vosges mountains (France), the river Rhine and groundwater. Chemical Geology, 160(1–2), 139-158.

van der Meer, J.J., Menzies, J., Rose, J., 2003. Subglacial till: the deforming glacier bed. Quaternary Science Reviews, 22(15), 1659-1685.

Viers, J., Roddaz, M., Filizola, N., Guyot, J.-L., Sondag, F., Brunet, P., Zouiten, C., Boucayrand, C., Martin, F., Boaventura, G.R., 2008. Seasonal and provenance controls on Nd–Sr isotopic compositions of Amazon rivers suspended sediments and implications for Nd and Sr fluxes exported to the Atlantic Ocean. Earth and Planetary Science Letters, 274(3–4), 511-523.

Wadham, J., Hodson, A., Tranter, M., Dowdeswell, J., 1998. The hydrochemistry of meltwaters draining a polythermal ‐ based, high Arctic glacier, south Svalbard: I. The ablation season. Hydrological Processes, 12(12), 1825-1849.

Walder, J.S., Fowler, A., 1994. Channelized subglacial drainage over a deformable bed. Journal of Glaciology, 40(134), 3-15.

Weis, D., Kieffer, B., Maerschalk, C., Barling, J., De Jong, J., Williams, G.A., Hanano, D., Pretorius, W., Mattielli, N., Scoates, J.S., 2006. High‐precision isotopic characterization of USGS reference materials by TIMS and MC‐ICP‐MS. Geochemistry, Geophysics, Geosystems, 7(8).

Weldeab, S., Emeis, K.-C., Hemleben, C., Siebel, W., 2002. Provenance of lithogenic surface sediments and pathways of riverine suspended matter in the Eastern Mediterranean Sea: evidence from 143 Nd/144 Nd and 87 Sr/86 Sr ratios. Chemical Geology, 186(1), 139-149.

Xu, J., Grumbine, R.E., Shrestha, A., Eriksson, M., Yang, X., Wang, Y., Wilkes, A., 2009. The melting Himalayas: cascading effects of climate change on water, biodiversity, and livelihoods. Conservation Biology, 23(3), 520-530.

Xu, Y., Simpson, A.J., Eyles, N., Simpson, M.J., 2010. Sources and molecular composition of cryoconite organic matter from the Athabasca Glacier, Canadian Rocky Mountains. Organic Geochemistry, 41(2), 177-186.

Yang, S., Jiang, S., Ling, H., Xia, X., Sun, M., Wang, D., 2007. Sr-Nd isotopic compositions of the Changjiang sediments: Implications for tracing sediment sources. Science in China Series D: Earth Sciences, 50(10), 1556-1565.

Figures:

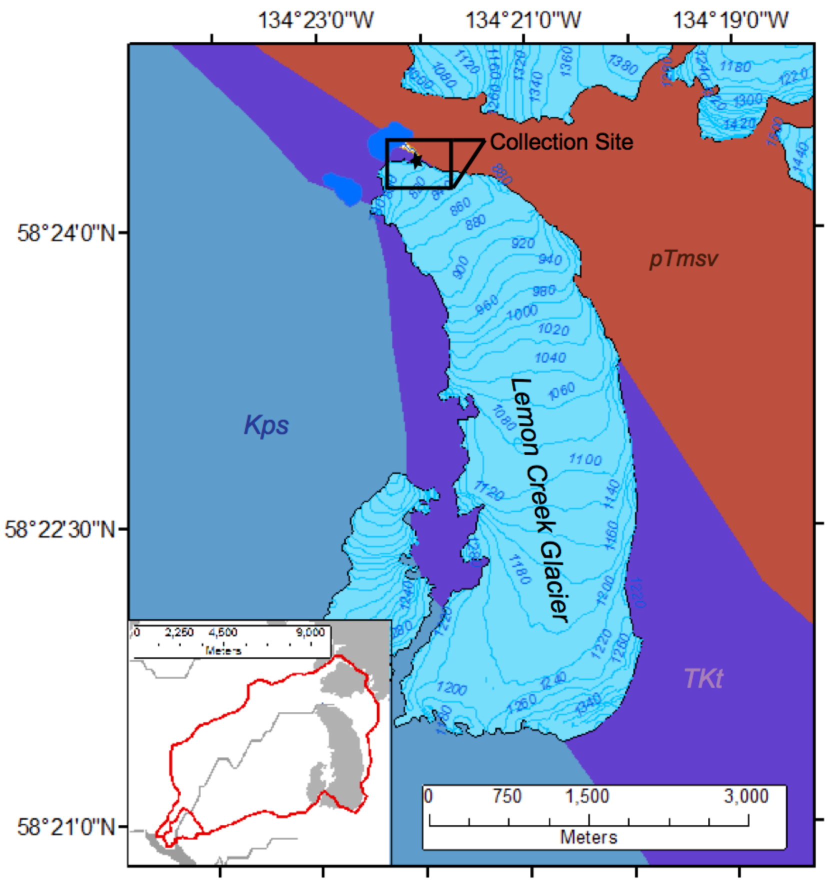

Figure 1: Modified from Stevenson et al. (In review) and provides geologic context of the Lemon Creek Glacier (LCG). Kps = Taku Terrane, composed of Greenschist facies and metamorphosed sedimentary rocks, Late Permian. TKt = Taku terrane, tonalite sills (62-69 Ma). pTmsv = Yukon-Tanana Terrane, high grade metamorphosed sedimentary and volcanic rocks, Carboniferous (Gehrels et al., 1984; Kistler et al., 1993; Samson et al., 1990). The inset depicts the Lemon Creek watershed, which extends to the Gastineau Channel and to the Gulf of Alaska. The watershed was delineated using USGS HydroSHED digital elevation maps (Lehner et al., 2008). The topographic lines represent 10 m of elevation on the LCG.

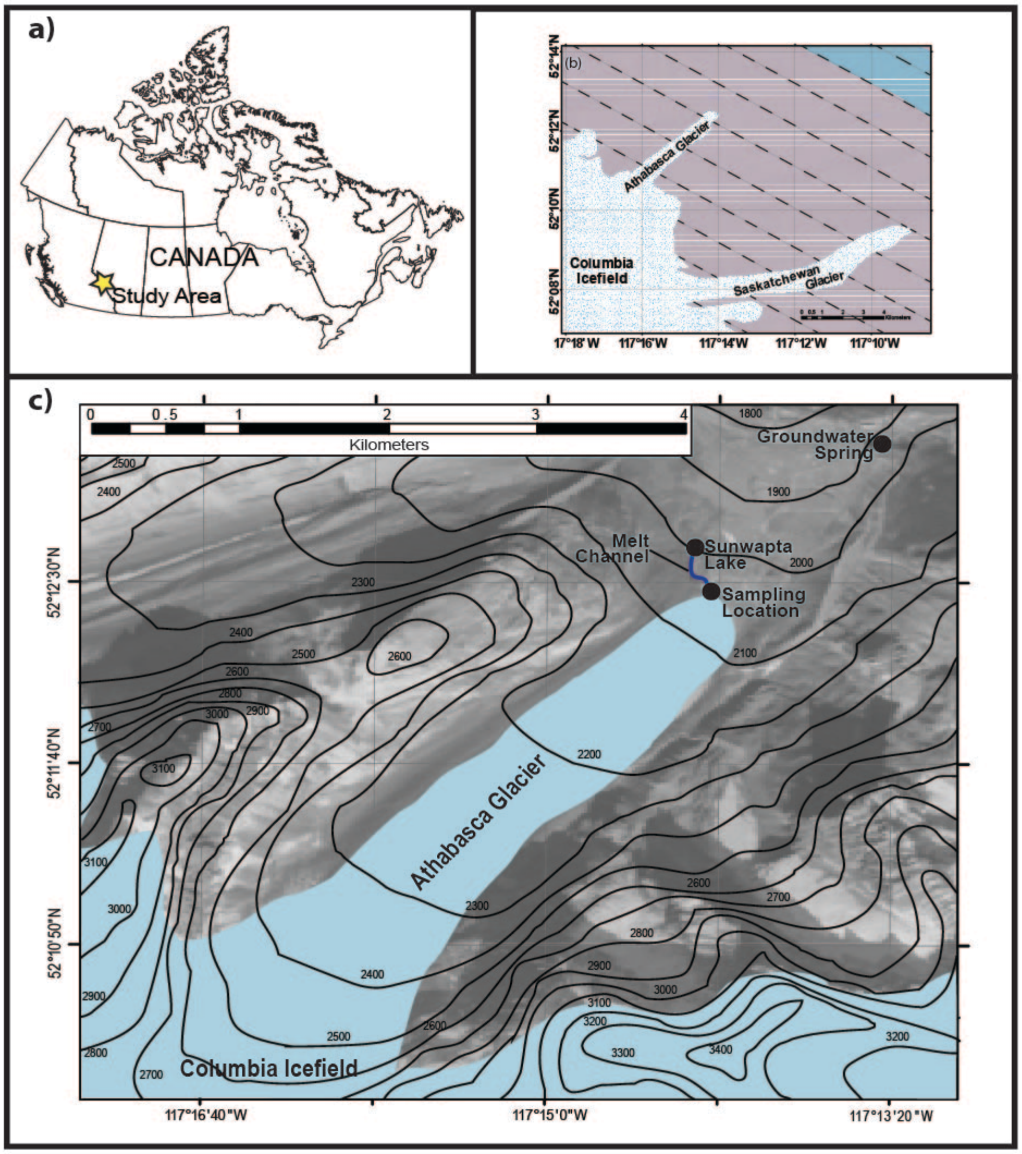

Figure 2: Modified from Arendt et al. (2015). Frames A and B show the geographic context and lithography, respectively, of the Athabasca Glacier (AG). The AG is primarily underlain by Middle Cambrian limestone and shale with the oldest rocks in the southwest, or increasing distance from the toe of the AG, and are indicated by the purple section. The oldest rocks are indicated in blue and the dashed lines represent rotation of the AG bedrock during formation. Frame C provides an elevation profile and detailed plot of the sampling location.

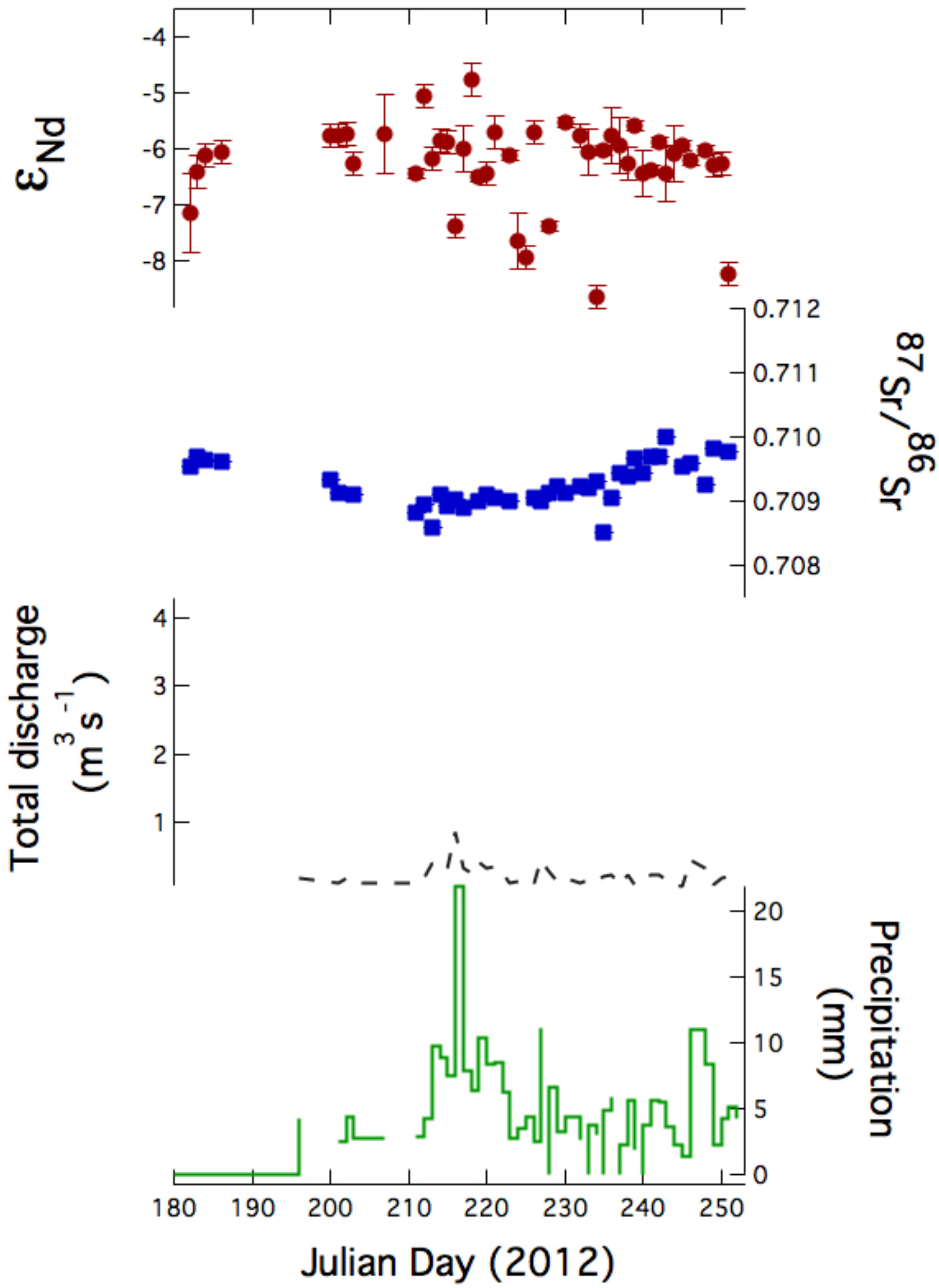

Figure 3: Time-series measurements from the Lemon Creek Glacier (LCG). The upper panels represent radiogenic neodymium (written in ε_{Nd}; red circles) and strontium (blue squares) values of the suspended sediment. Two standard errors are included. The lower panels depict seasonal trends of total discharge (black dashed line) and precipitation (solid green line).

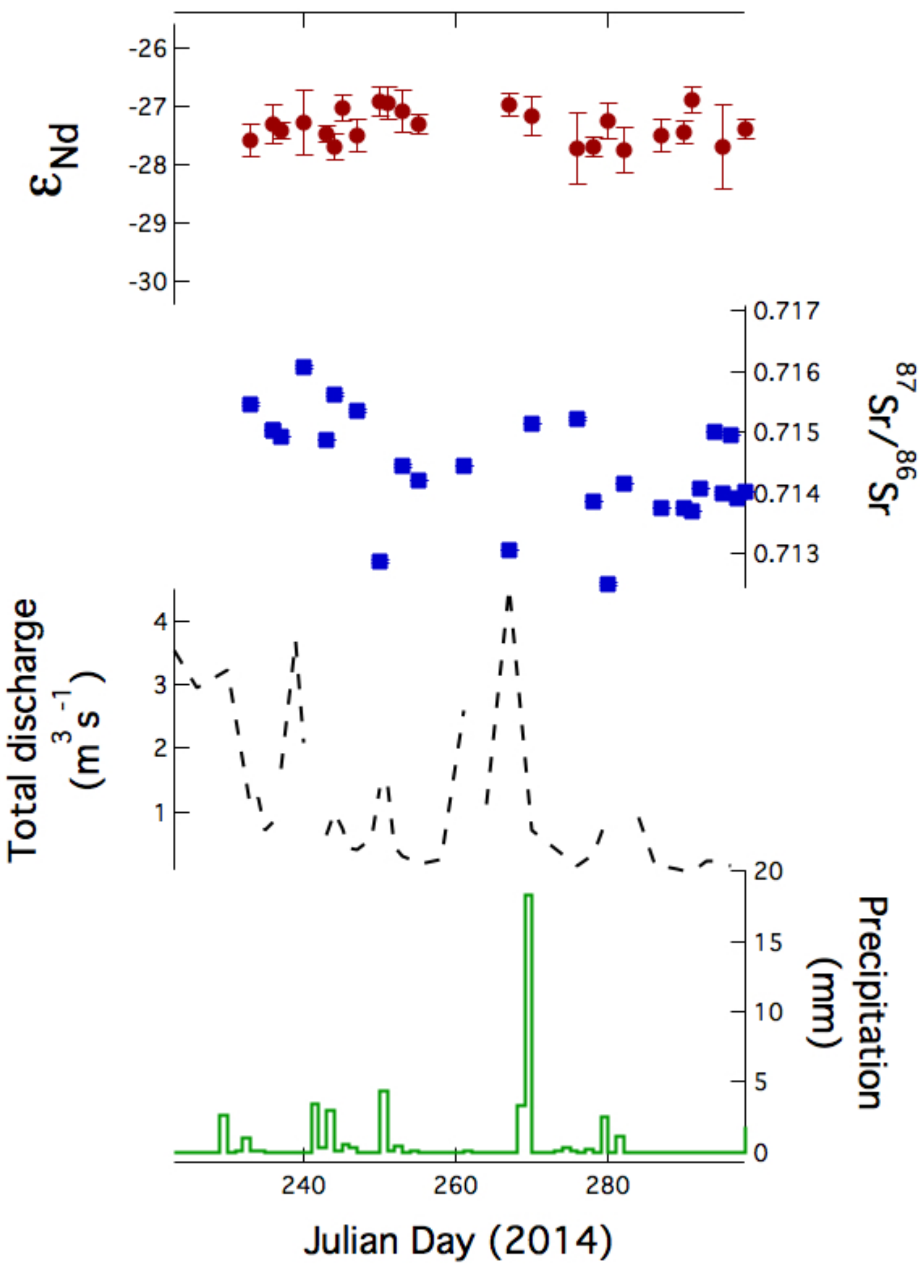

Figure 4: Time-series measurements from the Athabasca Glacier (AG). The upper panels represent radiogenic neodymium (written in ε_{Nd}; red circles) and strontium (blue squares) values of the suspended sediment. Two standard errors are included. The lower panels depict seasonal trends of total discharge (black dashed line) and the daily precipitation (solid green line).

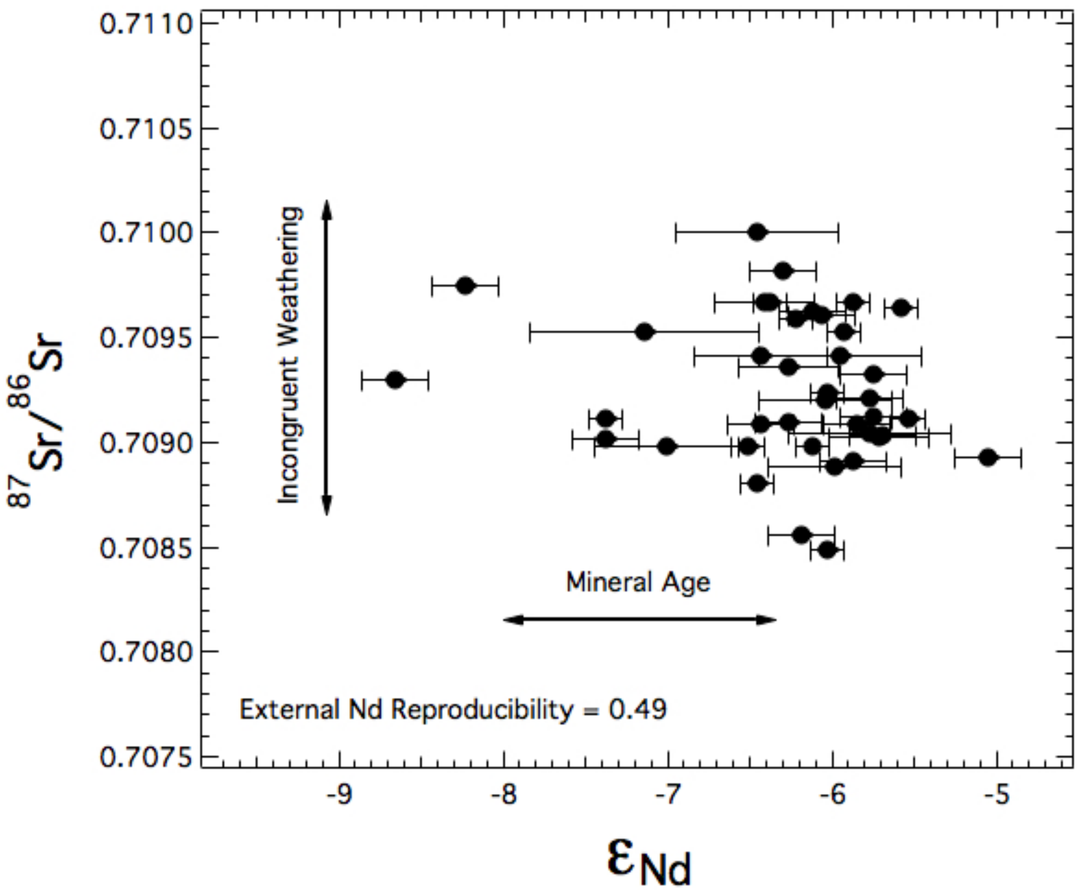

Figure 5: Correlation between $^{87}Sr/^{86}Sr$ and ε_{Nd} in the suspended sediment at the Lemon Creek Glacier. The error bars represent two standard error. The large range of ε_{Nd} ($\varepsilon_{Nd\ (Range)}$ ~4 units) at the LCG relates to a wide range of sediment mineral ages and suggests that the sediment is poorly mixed.

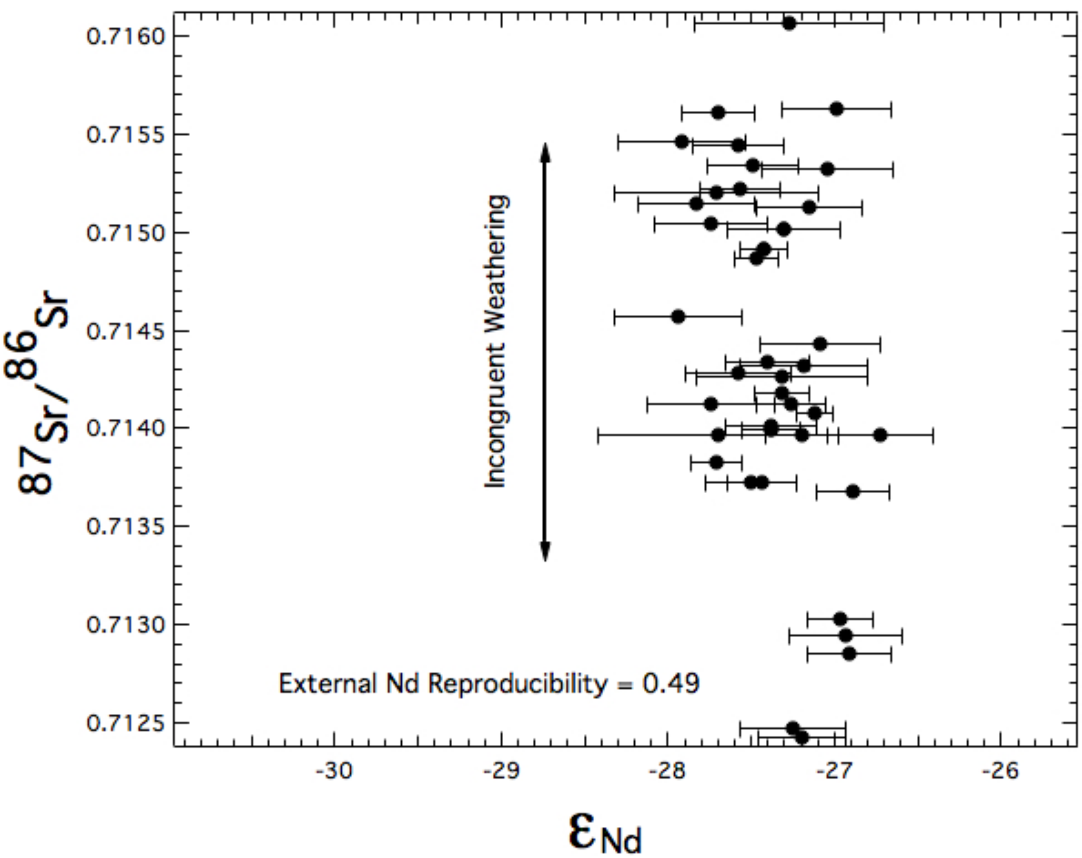

Figure 6: Correlation between $^{87}Sr/^{86}Sr$ and ε_{Nd} in the suspended sediment at the AG. Low variability is observed in the ε_{Nd}, with the included external reproducibility of $\varepsilon_{Nd} = 0.49$. The narrow range of ε_{Nd} ($\varepsilon_{Nd\ (Range)}$ ~2 units) at the AG suggests suspended sediment is well-mixed with regards to sediment age and variation is due to incongruent weathering processes.

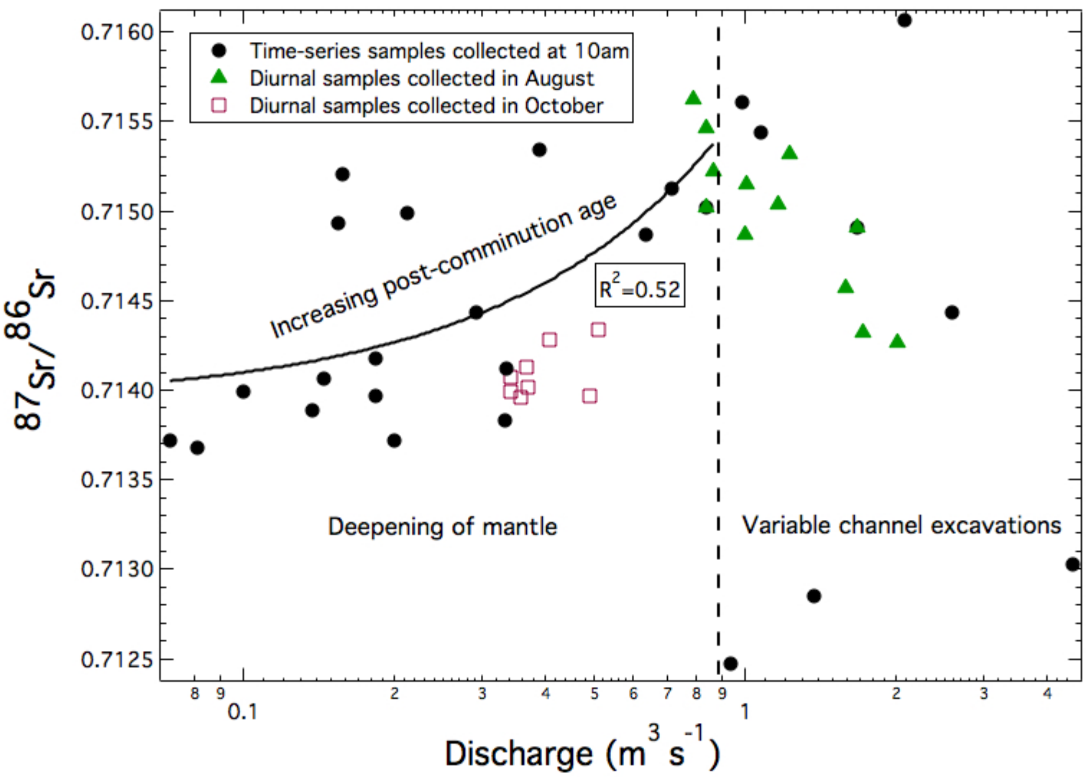

Figure 7: Correlation between $^{87}Sr/^{86}Sr$ ratio of the suspend sediment and total outflow discharge at the AG. Comminuted sediment mantles the bedrock with the greatest post-comminution age (i.e. greatest $^{87}Sr/^{86}Sr$ ratio) at the bedrock-sediment interface. At low discharge levels, the mantle is progressively deepened with increasing meltwater volumes. However, once a critical discharge level is reached (~0.9 $m^3 s^{-1}$), sediment excavation is non-discriminatory and the wide range of $^{87}Sr/^{86}Sr$ ratios can relate to processes such as exposure of previously isolated cavities.

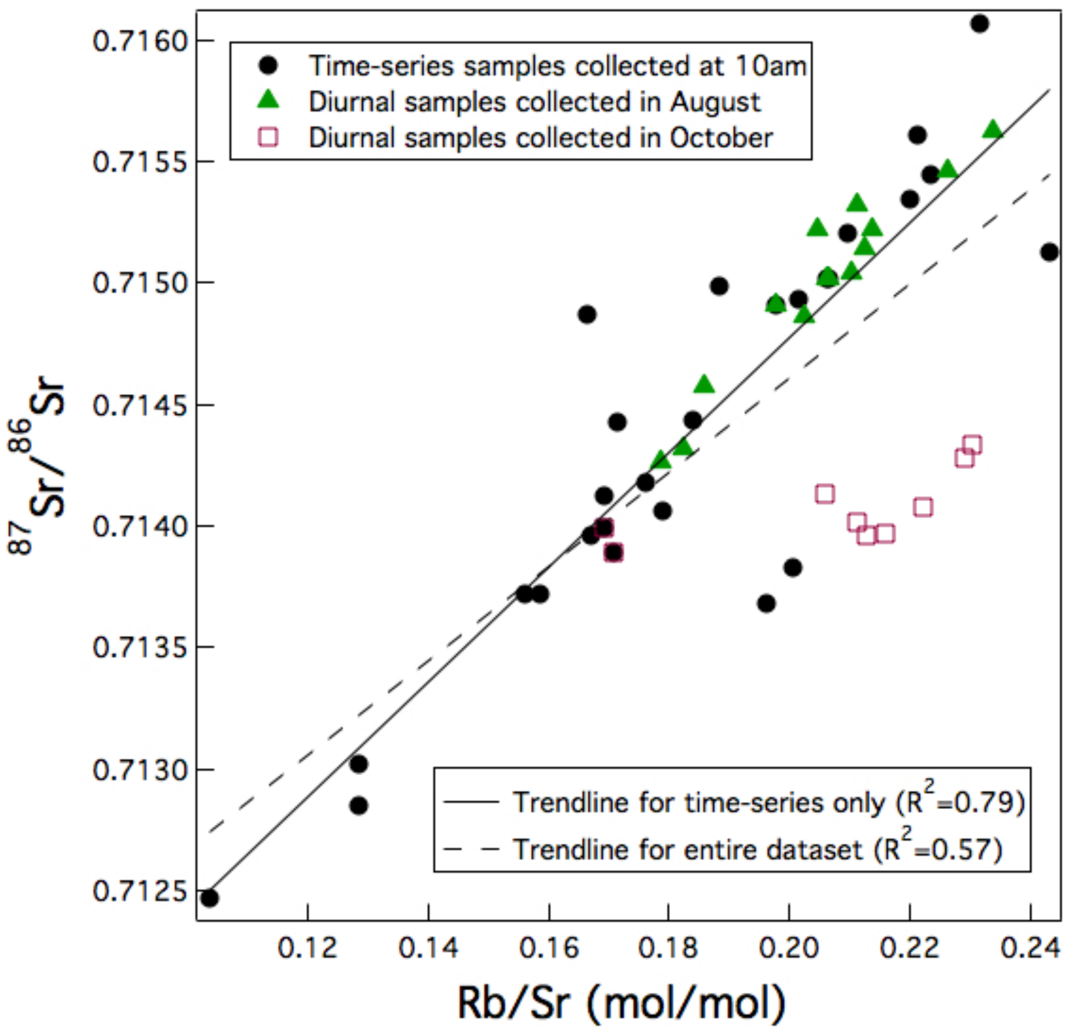

Figure 8: Plot relating $^{87}Sr/^{86}Sr$ and Rb/Sr ratios. A stronger correlation exists between the time-series measurements (R^2=0.79) in comparison to the complete dataset which includes both diurnal sample sets (R^2=0.57).

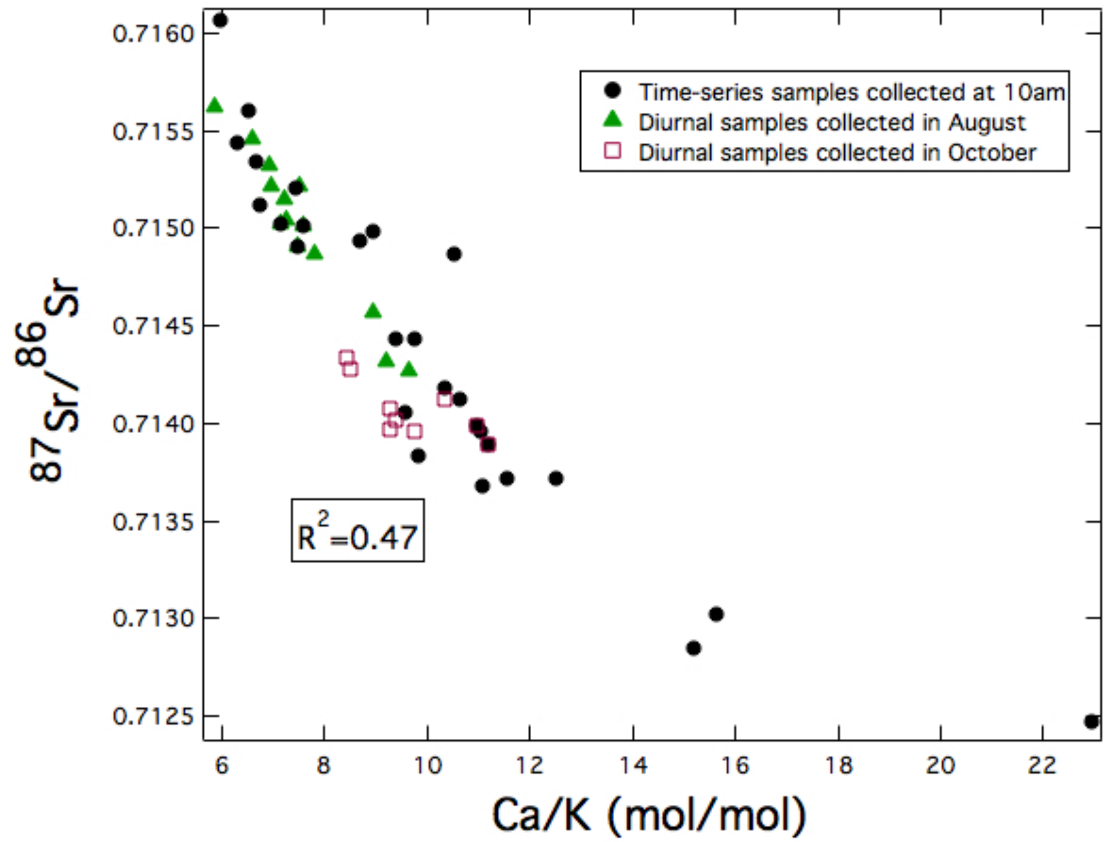

Figure 9: Relationship between $^{87}Sr/^{86}Sr$ and Ca/K in suspended sediment of the AG. Despite the predominately carbonate bedrock, the inverse relationship suggests preferential release of low $^{87}Sr/^{86}Sr$ bearing minerals during the initial stages of carbonate weathering followed by the release of higher $^{87}Sr/^{86}Sr$ bearing minerals during silicate weathering.

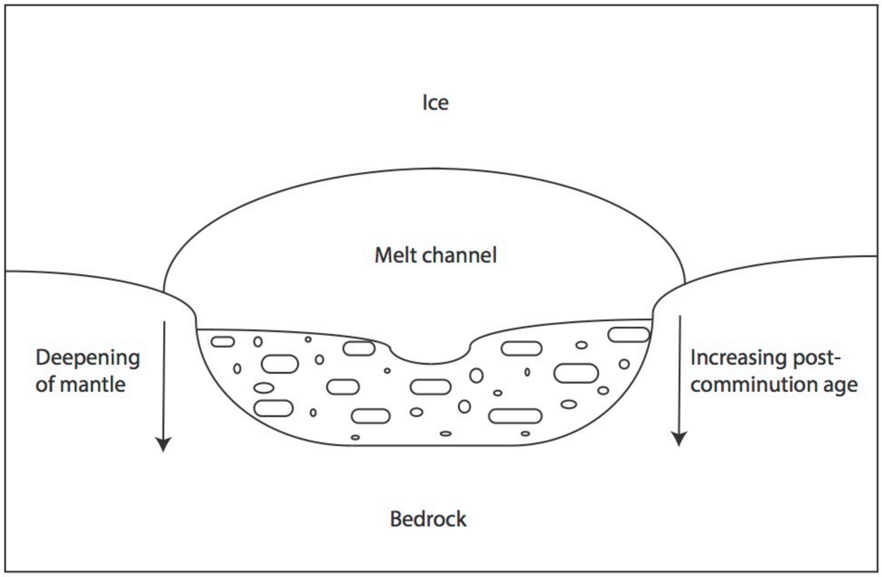

Figure 10: Simplified diagram of the deepening of the subglacial mantle with increasing meltwater excavating the comminuted sediment from the channel.

Supporting Online Material: Appendices 1 and 2 present the hydrophysical data and Appendices 3 and 4 present the isotopic data of the Lemon Creek Glacier and Athabasca Glacier, respectively. Additional figures provide support for the use of the coupled Nd-Sr proxy. Figure 11 depicts the correlation between the Sm/Nd and discharge of the suspended sediment at the AG and Figure 12 plots the ε_{Nd} and Ca/K of the suspended sediment at the AG. External reproducibility of 0.49 is included. The lack of correlation between K^+-bearing minerals (e.g. biotite, clays) indicates there is no trend between the age of the sediment and excavation processes, which further suggests the suspended sediment was well-mixed prior to the deposition of comminuted sediment.